Genetic background influences the phenotypic penetrance by MAFA^{S64F} MODY in male mice.

Zachary Loyd^{1,*}, Dongsoo Lee^{1,*}, Mallory Maurer¹, Lizabeth Buzzelli^{1,2}, Jin-Hua Liu², Min Guo², Garrett Reynolds², Mark A. Magnuson², Mark P. Keller³, Jean-Philippe Cartailler^{2,4}, Roland Stein², Jeeyeon Cha^{1,2,5,§}

¹Division of Diabetes, Endocrinology, and Metabolism, Department of Medicine, Vanderbilt University Medical Center, Nashville, TN, USA

²Department of Molecular Physiology and Biophysics, Vanderbilt University, Nashville, TN, USA

³Department of Biochemistry, University of Wisconsin-Madison, Madison, WI, USA

⁴Creative Data Solutions, Vanderbilt Center for Stem Cell Biology, Vanderbilt University, Nashville, TN, USA

⁵Veterans Affairs Tennessee Valley Healthcare System, Geriatric Research Education Clinical Center (GRECC), Nashville, TN, USA

*Co-first authors

§Corresponding author: jeeyeon.cha@vumc.org

ABSTRACT

Pancreatic β-cells require the coordinated expression of transcription factors such as MAFA to dynamically secrete insulin to maintain euglycemia. We previously identified that a naturally occurring mutation in MAFA (MAFA^{S64F}) predisposes carriers to divergent conditions of either maturity (adult)-onset diabetes of the young (MODY) or hypoglycemia in a sex-dependent manner, and we modeled these phenotypes in mice expressing this MafA variant. Here we show that the genetic background in mice can modulate penetrance of the male glycemic phenotype: heterozygous MafA^{S64F/+} males backcrossed on a C57/Bl6J ('C57') background prevents this pathology with improved insulin secretion, while MafA^{S64F/+} males on a mixed background (C57 with SJL) manifest overt diabetes and impaired insulin secretion by 5 weeks of age due (in part) to accelerated β-cell senescence. In contrast, female mice on either background (mixed or backcrossed C57) similarly show hypoglycemia. Bulk RNAseg on male C57/Bl6J islets revealed fewer differentially expressed genes (DEGs) and a more similar profile to MafAWT males than MafA^{S64F/+} males on the mixed background, including abrogation of β-cell senescence and intact expression of circadian regulators. CUT&RUN mapping revealed that MafA likely regulates several of the DEGs identified in both C57 and mixed genetic backgrounds. Our analysis also identified increased expression of many islet-enriched transcription factors directly regulating MafA expression (e.g., Pdx1) and increased MafA protein levels in C57 MafA^{S64F/+} males. In sum, these data suggest that the penetrance of diabetes caused MAFA^{S64F} activity in male human islet β-cells may be modulated by genetic background to impact β-cell senescence. circadian regulation, and islet function.

INTRODUCTION

MafA, the large V-Maf avian \underline{m} usculo \underline{a} poneurotic \underline{f} ibrosarcoma transcription factor (TF), is a pancreatic β-cell-enriched protein that is essential for activating transcriptional programs to promote β-cell maturation and function (1, 2). Compromised levels of mouse MafA (3-8) or human MAFA (9, 10) can impair β-cell function. For example, genetic knockout models of pancreatic MafA manifest impaired glucose tolerance in male and female mice (8), while human MAFA expression is reduced in islets recovered from donors with diabetes (9). Conversely, inducing MafA expression in normally non-glucose-responsive and MafA^{Low} neonatal rat islets increases β-cell function as defined by glucose-stimulated insulin secretion (GSIS) (11), and acute introduction of MAFA in mouse and human stem cells directly promotes insulin production and β-cell maturity markers (11-13), demonstrating a fundamental role for MafA in β-cell function and identity.

Pathogenic mutations in pancreatic islet-enriched TFs including MAFA can cause heritable, monogenic forms of islet dysfunction (*14*). Male carriers of a *MAFA* missense mutation (p.Ser64Phe, c.191C>T) develop sex-dependent diabetes, while female carriers of this mutation can develop persistent hyperinsulinemic hypoglycemia due to non-syndromic, insulinsecreting neuroendocrine tumors (insulinomatosis) (*15*). The resultant variant protein (termed MAFA^{S64F}) was found to impair phosphorylation of MAFA, which impacts not only its transcriptional activity but also dramatically increases protein stability: wild-type (MAFA^{WT}) has $t_{1/2}$ only ~30 minutes compared to many hours in MAFA^{S64F} (*15*). A mouse model harboring this clinically pathogenic mutation in the endogenous *MafA* gene (termed MafA^{S64F/+}) on a mixed genetic background (C57/Bl6J and SJL) mimicked the heterogeneous, sex-dependent phenotypes: female MafA^{S64F/+} mice were hypoglycemic, while male MafA^{S64F/+} mice shows impaired glucose tolerance due to widespread, premature β-cell aging and senescence (*16*). Introduction of this protein in male human β-cells also drove accelerated cellular aging (*16*), demonstrating conserved mechanisms of dysfunction.

Genetic background can profoundly influence diabetes penetrance (*17*), prompting our current study to backcross these mixed background mice to the C57/Bl6J ("C57") background. C57 was chosen since it is a known constituent of this mixed genetic background and historically well-characterized in metabolic studies as susceptible to glucose intolerance (*17*). Surprisingly, C57 MafA^{S64F/+} males show normal glucose tolerance compared to the overt diabetes of MafA^{S64F/+} males on a mixed background by 5 weeks of age, while no significant glycemic differences were demonstrated between MafA^{S64F/+} females of the two backgrounds.

Here, we evaluate differential molecular responses to the MafA S64F variant in males of these two strains. RNA sequencing on isolated male islets from both backgrounds revealed several differentially expressed gene (DEGs) impacting similar pathways, with reduced impairment in the C57 MafA MafA MafA CUT&RUN analysis suggests that MafA likely regulates the DEGs identified in both genetic backgrounds. In sum, these data suggest that clinical disease penetrance caused by the MODY MAFA S64F variant in male human β -cells may be modulated by genetic backgrounds.

METHODS

Mice

MafA^{S64F/+} heterozygous mice were originally generated using CRISPR/Cas9 targeting by the University of Michigan Transgenic Core on a mixed SJL and C57BL/6J mouse strain, as previously described (*16*). Mice were backcrossed eight generations with C57BL/6J mouse strain (Jackson Lab) to generate MafA^{S64F/+} mice on the C57 background ("C57"). These C57 MafA^{S64F/+} mice were crossed one time with SJL mice (Taconic) to reproduce a new mixed genetic background strain with largely 50:50 contribution of SJL and C57BL/6J ("Mixed") studied in this report. Proportional contributions of genetic backgrounds were confirmed by miniMUGA analysis (Transnetyx). Mice of both sexes were used in this study; details can be found in the results section and figure legends. All animal studies were reviewed and approved by the Vanderbilt University Institutional Animal Care and Use Committee. Mice were housed and cared for according to the Vanderbilt Department of Animal Care and the Institutional Animal Care and Use Committee of Animal Welfare Assurance Standards and Guidelines.

Intraperitoneal glucose tolerance testing and serum hormone measurements

Glucose tolerance testing was performed on MafA^{WT} and MafA^{S64F/+} mice (n = 6-16) in the afternoon given an intraperitoneal injection of D-glucose (2 mg/g body weight) prepared in sterile PBS (20% w/v) after a 6-hour fast (i.e. 8AM to 2PM). Insulin tolerance tests were conducted in the afternoon by intraperitoneal injection of 0.5 IU/kg body weight insulin (Novolin, regular human insulin, recombinant DNA origin) into mice (n = 3-5) fasted for 6 hours. Blood glucose was measured using a FreeStyle glucometer (Abbott Diabetes Care) before (0 minutes) and at 15, 30, 60, and 90 minutes following injection. Serum insulin and C-peptide was measured by Ultrasensitive Insulin ELISA (Mercodia) and C-peptide ELISA (Alpco), respectively.

Mouse islet isolation, RNA isolation, and gene expression analysis

Mouse islets were isolated using collagenase P (Sigma) injected into the pancreatic duct, followed by a Histopaque 1077 (Sigma-Aldrich) gradient. Islets were isolated and handpicked in standard RPMI-1640 medium (Thermo Fisher Scientific) supplemented with 10% FBS, L-glutamine, and penicillin-streptomycin, then frozen down in islet pellets. Islet RNA was then isolated using the RNAqueous Micro Total RNA Isolation Kit (Invitrogen). cDNA was generated using Superscript III reverse transcriptase (Invitrogen) by the oligo(dT) priming method. Real-time PCR assays were performed using the LightCycler FastStart DNA Master PLUS SYBR

Green kit (Roche) and a LightCycler PCR instrument (Roche). The real-time PCR primers are listed in **Supplemental Table 1**. Gapdh or β -Actin was used to normalize the data. Real-time PCR results were analyzed using the $\Delta\Delta$ Ct method (8).

Cell culture and RNA isolation

Monolayer cultures of MIN-6 mouse β -cells were grown under conditions described previously (4). Transfection with scrambled control, MAFA^{WT} or MAFA^{S64F} constructs of confirmed sequences (23) was performed using Lipofectamine 2000 (Invitrogen) (average transfection efficiency 80%) before protein or RNA isolation. RNA was isolated 4 days posttransfection using the Trizol reagent (Fisher Scientific). cDNA was generated using Superscript III reverse transcriptase (Invitrogen) by the oligo(dT) priming method. Real-time PCR assays were performed as above.

Western blotting

MAFA protein levels were normalized to endogenous β-actin by immunoblotting with anti-MAFA (Cell Signaling Technology, 79737) and anti–β-actin (MilliporeSigma, MAB1501) antibodies. Horseradish peroxidase–conjugated anti-rabbit (31460, Thermo Fisher Scientific) or anti-goat (31402, Thermo Fisher Scientific) secondary antibodies were used at 1:5000. Immunoblots were quantified with ImageJ (NIH).

Immunohistochemical analyses

Mouse pancreata were fixed overnight on ice in 4% paraformaldehyde (Electron Microscopy Services) in PBS, and pancreata were embedded in either Tissue-Plus OCT (Thermo Fisher Scientific) or paraffin wax. Sections of rodent pancreata were cut at 6μm thickness. The paraffin sections were deparaffinized and rehydrated before citrate buffer–based antigen retrieval. Sections were then made permeable by 0.5% Triton treatment for 10 minutes. Following blocking with 0.5% BSA in PBS for 120 minutes, the primary antibodies were applied overnight at 4°C. Primary antibodies are listed in **Supplemental Table 1**. Species-matched antibodies conjugated with the Cy2, Cy3, or Cy5 fluorophores were used for secondary detection (1:1000; Jackson ImmunoResearch). DAPI was used for nuclear staining (Southern Biotech). Immunofluorescence images were obtained using the Zeiss Axio Imager M2 widefield microscope with ApoTome.

Senescence-associated β-galactosidase (SA-β-gal) staining

Pancreata were snap frozen in O.C.T. and cryosections were prepared at 16μm thickness. SA-β-gal activity staining was performed at pH 6.0 (*16*) (Cell Signaling). To compare the intensity of SA-β-gal staining, sections from different genotypes and ages were processed on the same slide. Staining reactions were developed for 18 hours at 37°C, then quenched by 3x PBS washes (pH 7.4). Slides were then subject to immunostaining for insulin by fixing in 4% paraformaldehyde for 45 minutes, permeabilized with Tris-buffered saline with 0.2% Triton X-100 for 15 minutes, blocked in 2% normal donkey serum/1% BSA in PBS and incubated overnight with guinea pig anti-insulin (1:500, Fitzgerald 20-IP35) at 4°C. HRP-conjugated secondary antibodies were incubated on slides for 1 hour and detected with the DAB+ chromogen kit (DAKO). After washing, slides were mounted and imaged by brightfield microscopy.

RNAscope and quantification

MafA^{WT} and MafA^{S64F/+} pancreata from 5-week-old mice were harvested and fixed in 10% neutral buffered formalin for 72 hours. Tissues were embedded in paraffin wax, serially sectioned to 5μm thickness, and air dried for 10-14 days prior to processing. The RNAscope® Multiplex Fluorescent Reagent Kit V2 (ACD) was used following manufacturer's instructions. In short, pancreas sections were incubated at 60°C for one hour, then deparaffinized with xylene, dehydrated, and incubated for an additional 30 minutes. Tissues were treated with hydrogen peroxide for 10 minutes and placed in 1X target retrieval solution (ACD) at 100°C for 15 minutes. Sections were then treated with Protease Plus in ACD HybEZ™ II Oven at 40°C for 30 minutes. Afterward, the sections were incubated with *Cdkn1a* C-1 probe (ACD) at 40°C for 2 hours, followed by 3 amplification steps of 30, 30, and 15 minutes. The probes were visualized with the Opal fluorophores. Co-immunostaining for Insulin protein was performed using guinea pig anti-insulin antibody (Fitzgerald 20-IP35). Cy-2 conjugated secondary antibody and DAPI were incubated on the slides for 1.5 hours. After PBS washes, slides were mounted using Prolong Gold Antifade Mountant (Invitrogen) and imaged on the Leica DMi8 inverted microscope at 40X objective.

RNAscope images were analyzed using QuPath (24). Regions of interest (ROI) around islets were defined based on insulin staining positivity. Stardist(25), a deep-learning-based nuclei detection model, was used to detect nuclei and outline the cell via a cell expansion of 2.5 µm. Max entropy or triangle auto-threshold methods and image down-sampling (factor of 2) was used to determine the threshold for each channel with an RNA probe. RNA speckles were

detected using the subcellular detection feature in QuPath with the calculated thresholds. Percentage of β -cells positive for Cdkn1a was calculated in QuPath and exported to Prism for statistical analysis.

Bulk RNASeq and analysis of mouse islet cells

Bulk RNA-Seq was performed on MafA^{S64F/+} mouse islets isolated at 5 weeks of age.

RNAqueous Micro Total RNA Isolation Kit (Invitrogen) was used to isolate total RNA, and RNA quality was analyzed on an Agilent 2100 Bioanalyzer. Samples with RIN >8 were used for sequencing. The cDNA libraries were constructed, and paired-end sequencing was performed on an Illumina NovaSeq6000 (150-nucleotide reads). The generated FASTQ files were processed and interpreted using the Genialis visual informatics platform

(https://www.genialis.com) as described previously(16). DESeq2 was used for differential gene expression analyses and statistical comparison, as previously described (26). Poorly expressed genes, which have expression count summed over all samples below 10, were filtered out from the differential expression analysis input matrix. Sequencing data were deposited in the National Center for Biotechnology Information (NCBI) Gene Expression Omnibus (GEO) database (accession no. GSE299343)

CUT&RUN assay and analysis

CUT&RUN was performed on 500,000 dispersed mouse MIN6 cells per condition using CUTANA ChIC/CUT&RUN protocol v3.1 (Epicypher). Nuclei were extracted with nuclear extraction buffer (20 mM HEPES-KOH [pH 7.9]; 10 mM KCl; 0.1% Triton X-100; 20% glycerol; 1 mM MnCl2; 0.5 mM spermidine; 1uM protease inhibitor; Thermo Fisher Scientific) for 10 minutes on ice and immobilized onto Concanavalin-A beads (EpiCypher). After blocking and washes, samples were incubated with 0.5 µg of rabbit anti-MAFA (Cell Signaling 79737) or rabbit anti-IgG (EpiCypher 13-0042) antibodies overnight at 4°C. pAG-MNase (EpiCypher) was added to nuclei (1:20) and incubated at room temperature for 10 minutes. Targeted chromatin digestion was induced by adding 100 mM CaCl₂ and nutating for 2 hours at 4°C. DNA fragments were purified using the CUTANA ChIC/CUT&RUN kit, according to the manufacturer's instructions. DNA was resuspended in 0.1M~ Tris-EDTA buffer solution and used for library preparation with the CUTANA CUT&RUN Library Prep Kit (EpiCypher, 14-1001), according to the v1 manual. Libraries were sequenced as PE150 reads on the NovaSeq platform. All libraries had > 15 million reads. and were processed using the nf-core/cutandrun workflow, v3.1 (27). The pipeline performs adapter trimming, alignment to the GRCm38 reference genome, filtering

against the mm10 blacklist regions, spike-in normalization, and peak calling using MACS2. The workflow also generates IGV sessions and all track data, which allows for interactive visualization and exploration. Quality was confirmed by fragment length distribution and fingerprint plots. Nearest gene analysis was performed with peakScout (28). Coverage plots were created using ggcoverage (29). Sequencing data were deposited in the National Center for Biotechnology Information (NCBI) Gene Expression Omnibus (GEO) database (accession no. GSE298664).

Genetic background SNP analysis. We used the single nucleotide polymorphism (SNP) search tool at MGI (https://www.informatics.jax.org/snp) to identify all SNPs that are polymorphic between C57BL/6J and SJL/J. To annotate these SNPs and their predicted consequence we utilized the Variant Effect Predictor (VEP) tool (v114.0) (30), which allowed us to recover several variant classes associated with coding and no-coding genomic regions. We further leveraged comprehensive annotations available from the Ensembl and GENCODE databases to predict the functional consequences of the annotated SNPs.

Statistical Analysis. Data are expressed as the mean ± SEM. Statistical analysis was performed using GraphPad Prism 9.5.0 (GraphPad Software Inc.). The differences between groups were analyzed by unpaired 2-tailed Student's t test or 2-way ANOVA, as indicated. Differences were considered to be statistically significant at P < 0.05.

RESULTS

Glucose tolerance is largely unaffected in MafA^{S64F/+} males on a C57 background, while those on a mixed background manifest overt diabetes and impaired insulin secretion.

We previously identified heterogenous phenotypes in response to the MafA^{S64F} variant in male and female mice on a mixed genetic background (C57/Bl6J and SJL) (*16*). Mutant mice of both biological sexes showed improved glucose tolerance at birth, then diverged in phenotype beginning at 5 weeks of age: impaired glucose tolerance was demonstrated in MafA^{S64F/+} males while MafA^{S64F/+} females showed persistently mild hypoglycemia. We backcrossed these mice to a C57/Bl6J (C57) genetic background, and strikingly, dysglycemia of male MafA^{S64F/+} mice was prevented (**Fig. 1A**). We decided to breed this C57 MafA^{S64F/+} line with SJL mice (purchased from Taconic) to produce an F1 generation which recovered the frank dysglycemia in the MafA^{S64F/+} males (**Fig. 1B**)(*16*). These mixed background F1 mice showed impaired insulin and C-peptide secretion (**Fig. 1C-D**), compared to intact C-peptide secretion in the C57 MafA^{S64F/+} males (**Fig. 1E**). Interestingly, the hypoglycemia phenotype of MafA^{S64F/+} females remained consistent between the genetic backgrounds (**Fig. 2A-B**), with either intact (mixed background) or improved (C57 background) *in vivo* insulin and/or C-peptide secretion (**Fig. 2C-E**).

We previously reported that MafA^{S64F/+} males show transient hypoglycemia preceding impaired glucose tolerance at 5 weeks of age (*16*). Random glucose levels of 2-3 week old pups on the mixed background showed relative hypoglycemia preceding dysglycemia in the male mutant mice, similar to the female mutant mice (**Supp Fig. 1A**) (*16*). We recognized that the time of phenotype onset between 4 and 5 weeks of age coincided with weaning and a shift in dietary intake from nursing to chow pellets. Thus, we performed an extended wean protocol to evaluate glycemia of these mice while nursing. Even so, male mutant mice showed elevated random glucose levels compared to their wild type (WT) littermates (**Supp Fig. 1B**), demonstrating the dominant effects of the mutation on glycemia over dietary change. Weight gain as a proxy of overall health was not impacted by the mutation in either genetic background (**Supp Fig. 1C-D**), and peripheral insulin sensitivity was largely intact in all groups by insulin tolerance testing (**Supp Fig. 1E**). These results demonstrate heterogeneous impact of the MafA^{S64F} variant across biologic sex and genetic backgrounds, and that these effects are primarily mediated at the level of the pancreatic islet.

Islet senescence is abrogated in C57 MafA^{S64F/+} male islets compared to those from mixed MafA^{S64F/+} males.

Since glycemic phenotypes were markedly different between MafA^{S64F/+} males, but not females. across the two genetic backgrounds (i.e., Mixed and C57), we focused our remaining analysis on the males to better understand protective and diabetogenic influences of the C57/Bl6J and SJL backgrounds, respectively. Accelerated senescence is a feature of islets from T1D and T2D donors, which can be recapitulated in mouse models of diabetes such as those with insulin resistance modeling T2D (31), NOD mice modeling T1D (32), and in male MAFA^{S64F} MODY (16). As we reported previously, accelerated cellular aging of islets was dominant in MafA^{S64F} males on a mixed background with islet enrichment of senescence associated-β-galactosidase (SA-β-gal) staining and expression of known senescence markers, including those in the DNA damage response pathway and senescence-associated secretory phenotype (16). While these changes were confirmed in the mixed background MafA^{S64F/+} mice (**Fig. 3A**), they were not evident in the MafA^{S64F/+} male islets from a C57 background (Fig. 3B). In particular, the Cdkn1a encoding p21, implicated as a principal driver of cell cycle arrest and β-cell senescence (33), was enriched in MafA^{S64F/+} males on a mixed, but not C57, background (Fig. 3C). Moreover, markers of DNA damage and impaired nuclear integrity (seen in islet senescence) (33) were enriched in male mutant islets from the mixed, but not C57, background (Fig. 3D-E). As expected, islet senescence signatures are not seen in female Het islets of either background (Supp Fig. 2A-B).

Unbiased RNASeq analyses demonstrates improvement of senescence signatures in C57 MafA^{S64F/+} males compared to mixed background MafA^{S64F/+} males.

We next took an unbiased approach to further evaluate the molecular differences between the MafA^{WT} and MafA^{S64F/+} males of mixed and C57 genetic backgrounds showing dysglycemia and its genetic rescue, respectively. We isolated male islets of each background at 5 weeks of age (age of phenotype onset, **Fig. 1B**). Islet recovery was markedly reduced in MafA^{S64F/+} mice of a mixed background as we had seen previously (*16*), but recovery was grossly improved from C57 Het males, at comparable yields to littermate control males (**Fig. 4A**). We performed bulk RNASeq to assess dominant gene expression patterns between these groups. Unbiased clustering identified that the molecular signatures between MafA^{WT} and MafA^{S64F/+} males on a C57 background were more similar than between MafA^{WT} and MafA^{S64F} male islets on a mixed background (**Fig. 4B**). Differentially expressed genes were then evaluated: MafA^{S64F/+} mice of C57 background had 2,097 differentially expressed genes (DEGs) (616 up and 1481 down) compared to male WT islets on this background, while MafA^{S64F/+} mice of mixed background had

more DEGs than the C57 background (3,366: 1505 up and 1861 down) (**Fig. 4C**). Of these, only 386 upregulated and 621 downregulated DEGs were similarly impacted between the backgrounds. We evaluated senescence-associated gene expression (i.e., aging, DNA damage, SASP, and senescence composite signatures) and found them to be enriched in the MafA^{S64F/+} males in both backgrounds, but with increased enrichment in the mixed background (**Fig. 4D**).

RNASeq analysis also revealed novel gene expression differences between genetic backgrounds, including those regulating β -cell identity and circadian rhythm

We then evaluated DEGs of MafA^{S64F/+} males that were unique to each genetic background (i.e. 855 downregulated and 228 upregulated in the C57 MafA^{S64F/+} background males, vs. 1238 downregulated and 1114 upregulated in the MafA^{S64F/+} mixed background males) to determine unique pathways affected in each background in response to the MafA variant (**Fig. 4C**). Gene Ontology analysis of the DEGs identified enrichment of similar pathways involved in pancreatic exocrine secretion, protein digestion and absorption, calcium signaling pathways (**Fig. 5A**), all previously associated with cellular aging (*16*), in both backgrounds. However, this enrichment was muted in the C57 males compared to mixed background males (**Fig. 5A**).

Downregulated pathways specifically in the C57 background included nuclear receptors in lipid metabolism and retinol metabolism (Fig. 5A). In contrast, downregulated pathways in the mixed background included neuroactive ligand-receptor signaling components such as Somatostatin (Sst) and neuropeptide Y (Npy), both known to have modifying effects on pancreatic β-cells and differentiation (34, 35). Circadian entrainment was also downregulated in mixed background mutant islets. Indeed, entrainment of islet β-cells is essential for optimal βcell function (36, 37), and oscillatory insulin secretion is synchronized with nutritional intake and expression of genes encoding insulin secretory machinery and signaling factors to regulate insulin secretion (36, 38-40). STRING analysis (41) of the DEGs unique to each genetic background was performed to further evaluate function by protein association networks. Networks significantly changed in MafA^{S64F/+} mixed background males again demonstrated protein digestion, calcium signaling, neuroactive ligands (such as Sst, Npy), and circadian entrainment (Fig. 5B). Taken together, these results suggest that common pathways such as senescence are similarly enriched (albeit at lower significance in the C57 background) between the two backgrounds, however, each background showed impairment in unique pathways in response to the variant.

MafA directly bind and regulate the expression of genes involved in circadian entrainment.

We were intrigued by the novel association with diminished circadian regulation unique to mixed background MafA^{S64F/+} males. Peripheral circadian clocks are evident across metabolic tissues and differ from the primary clock of the hypothalamic suprachiasmatic nucleus in that entrainment occurs, not only by light itself, but by a number of hormonal, autonomic and physiologic inputs, including those signals generated by fasting/feeding cycles (42). The mammalian circadian clock core proteins Clock and muscle ARNT-like 1 (Bmal1) function as a heterodimer (Clock:Bmal1) to drive rhythmic behavior, metabolism, and gene expression in all metabolic tissues, including the pancreatic islet (43). Periodicity of Clock:Bmal1 activity is regulated by autoregulatory loops driven by their own transcriptional targets serving as repressors, such as Period1/2 (Per1/2), Crytochrome1/2 (Cry1/2), (43). The rhythmic and diurnal β-cell expression of Per1, Per2, Cry1, and Cry2, along with regulators in parallel pathways which can either amplify and repress these signals such as nuclear receptor subfamily 1 group D member 1 (Rev-erba), RAR-related orphan receptor alpha (Rora), basic helix-loop-helix family member (Bhlhe40/Dec1) and D-site albumin promotor binding protein (Dbp) (18, 39, 40, 42-46), sets up a highly effective feedback loop that promotes dynamic insulin secretion. In fact, disrupting local β-cell Clock:Bmal1 action can disrupt insulin secretion (18, 19) while inducing Bmal1 improves β-cell function (47). Moreover, human islets from diabetic donors show reduced expression of core clock elements such as Clock, Per1-3, Cry2, Rev-erba, and Dbp (21, 22).

Here, islet gene expression by RNASeq showed a generalized repression of the circadian regulators: repressors such as Cry1/2, Per1/2, Bhlhe40/Dec1, and Rev-erb, and modifiers such as Rora and Dbp, in the MafA^{S64F/+} males of the mixed background (**Fig. 5C**). Interestingly, the expression of core circadian activators Bmal and Clock remained similar between genotypes and genetic background, affirming that the genetic-background related dysregulation of circadian rhythms is related to turnover and degradation of the regulators rather than the core Clock:Bmal1 components themselves (*42*). Immune activation via NFkB can alter circadian rhythms by inhibiting these core clock repressors to regulate islet-enriched *Pdx1* expression (*36, 38*), however, MafA^{S64F/+} male islets did not show changes in nuclear (active) NFkB localization by immunostaining, suggesting an NFkB-independent mechanism in mixed background MafA^{S64F/+} males (**Supp Fig. 3A-B**).

We then questioned whether the DEGs uniquely identified in each background were a target of the MafA transcription factor, or rather an indirect consequence of the variant protein. Thus, we performed CUT&RUN analysis (27) to identify genome-wide regions of endogenous MafA occupancy in the mouse Min6 β -cell line, and peaks were annotated by nearest gene (n=11,403 peaks identified) (**Fig. 6A**).

We then overlaid these gene-annotated MafA CUT&RUN peaks with the DEGs uniquely identified in MafA^{S64F/+} males of each genetic background (**Fig. 6A**). This analysis yielded 250 DEGs which could be direct targets of MafA in the C57 background, which included factors in the senescence-associated prosurvival Bcl2 family (ie., Bcl2l14), Slit/Robo signaling (Robo3), and retinoic acid signaling (e.g., RAR α/β). Similar analysis in MafA^{S64F/+} male islets on a mixed background yielded 1210 potential targets. These included genes associated with β-cell identity and islet hormones such as urocortin 3 (Ucn3), glucagon (Gcg), somatostatin (Sst), cholecystokinin (Cck), insulin (Ins), and gastrin (Gast); islet-enriched transcription factors and receptors such as Glis1, Glp1r, Nkx6.2, Nkx6.3, Onecut1 and Smarca1; and circadian regulators Cry2, Per1, Per2, Rora, Dbp, Bhlhe40/Dec1, Nr1d1 (Rev-erba), Nr1d2 (Rev-erb) (examples in **Fig. 6B**). Notably, several core senescence mediators such as *Cdkn1a* (encoding p21), *Bcl2a1d*, *Ankrd1*, or *Icam1* (**Fig. 4D**), were not identified as MafA targets by CUT&RUN, suggesting that cellular aging may not be a direct transcriptional consequence of MafA^{S64F}.

C57 MafA^{S64F/+} male islets show improved expression of known MafA targets, and differential SNP analysis between C57 and SJL genetic backgrounds predict differences in expression of MafA interacting proteins.

Compared to frankly impaired expression of known MafA target genes on the mixed background, MafA^{S64F/+} male islets on the C57 background show muted gene expression changes of known targets, such as Ins1, Ins2, Pdx1, Glp1r, and Gck (**Supp Fig. 4A**) (*1*). We expect that the binding ability of MafA^{S64F} to be similar to the MafA^{WT} protein since the mutation does not impact the DNA binding region. As proof of principle, gel shift assay showed that MafA^{WT} or MafA^{S64F} transfected in HeLa cells showed similar binding ability to target regions such as the *Insulin1* enhancer (**Supp Fig. 4B**). Thus, we investigated whether the expression of known MafA co-regulators which modulate MafA activity are distinct between the backgrounds. We found only subtle expression differences between C57 and mixed background Het mice of known coregulators (**Supp Fig. 4C**).

We also used the single nucleotide polymorphism (SNP) search tool at MGI (https://www.informatics.jax.org/snp) to identify SNPs that are polymorphic between C57BL/6J and SJL/J associated with coding and no-coding genomic regions. We further leveraged comprehensive annotations available from the Ensembl and GENCODE databases to predict the functional consequences of the annotated SNPs. We identified ~5,260 unique C57BL/6J vs. SJL/J polymorphic SNPs. Of these, 566 unique SNPS were found to occur within 18 genes encoding known MafA interacting proteins (Supplemental Table 2), which included: Creb1 (n=220 unique SNPS), Dpy30 (n=12), Fam8a1 (n=1), Hnf1a (n=1), Kat2b (n=107), Kdm6b (n=3), Map3k7 (n=25), Mbip/Map3k12 binding protein (n=9), Ncoa6 (n=70), Nkx2.2 (n=37), Onecut1 (n=6), Pias4 (n=1), Pole4 (n=15), Rbbp5 (n=6), Rnf145 (n=9), Tada3 (n=16), Ube2j1 (n=27), and Usp7 (n=1). No SNPs were predicted to result in a missense variant of MafA interacting protein or within MafA itself (Supplemental Table 3). Collectively, these results suggest that additive effects of small differences in multiple coregulators may contribute to differential MafA activity across genetic backgrounds, but this requires further investigation.

MafA phosphorylation status is partially preserved in C57 MafA^{S64F/+} male islets.

MafA activity is also dependent upon its posttranslational modifications (1). MafA^{WT} is highly modified by phosphorylation to couple two antagonistic regulatory processes: increased transactivation activity *and* ubiquitin-mediated degradation (*48*), This demonstrates that impeccable regulation of this protein is linked to islet β-cell health. MafA^{S64F} shows impaired phosphorylation, converting the normally unstable MAFA protein ($t_{1/2} \sim 30$ min) to a remarkably stable one ($t_{1/2}$ on the order of several hours) (*15*). In vivo, autoregulation of MafA expression results in profound downregulation of the MafA transcript and β-cell mass (*16*). Indeed, differential SNP analysis identified genes reported to either regulate MafA transcriptional expression (e.g., Creb1, Nkx2.2, Onecut1) (*49-51*) or are involved with protein ubiquitination for protein degradation (e.g., Rnf145, Ube2j1, Usp7) (*52-54*) (**Supplemental Table 3**).

We found that MafA presence was markedly reduced in mixed background, but not C57 background (**Fig. 7A-B**) in male Het islets. As these mice are heterozygous for the mutant MafA allele, we questioned whether MafA^{S64F/+} males between the genetic backgrounds show differences in MafA^{S64F} abundance. Immunoblotting for MafA on isolated primary islets showed an increased presence of a fully phosphorylated (i.e., WT) MafA species in the C57 background, compared to a predominant underphosphorylated (i.e., S64F) band in the mixed background (**Fig. 7C**). Quantification of the bands confirmed the predominance of the underphosphorylated

MafA species in the mixed background compared to the C57 background, which showed relatively equal proportions of phosphorylated to underphosphorylated MafA (**Fig. 7D**).

MafA expression is largely intact in C57 MafA^{S64F/+} male islets.

Our prior work had also shown that MafA is downregulated at the transcript levels in islets isolated from MafA^{S64F} males the mixed background (16). Interestingly, we find relatively intact MafA transcript levels in islets of the MafA^{S64F/+} males the C57 background (**Fig. 8A**). This prompted us to evaluate transcriptional regulators of MafA across these backgrounds. By bulk RNAseq, we found that several MafA interacting islet-enriched factors were dysregulated across backgrounds (**Supp. Fig 4D**). Indeed, known MafA activators Pdx1 (50) was poorly expressed in the nuclei in the mixed, but not C57, background islets (**Fig. 8B**), while MafB (another islet-enriched family member) was aberrantly enriched in the C57 β -cells (**Fig. 8C**). In sum, these results link the profound differences in the glycemic phenotypes between genetic backgrounds with integrated differences in islet MafA expression, MafA^{S64F} variant abundance, and MafA activity for target gene expression.

DISCUSSION

Prior work has highlighted the therapeutic potential of strategies that can maintain MAFA levels in β-cells (2). A rare, naturally occurring missense mutation in the MAFA transactivation domain (S64F), which impairs posttranslational modifications necessary for ubiquitin-mediated degradation, profoundly increases the stability of the MAFA (15). However, carriers of this variant manifest sex-dependent glycemic disorders: men show maturity-onset diabetes while women moreso have hypoglycemia with non-syndromic insulinomatosis (15). Since this original report, a second MafA missense mutation in the transactivation domain have been identified in which carriers develop dysglycemia and is also predicted to promote MafA protein stability (55), confirming an unexpected pathogenicity of stabilizing MafA mutations and heterogeneity in clinical phenotypes.

A mouse model harboring the S64F mutation in the endogenous *Mafa* gene recapitulated the heterogenous, sex-dependent responses seen in patients (16), providing surprising insights into the impact of this MafA variant *in vivo*, including a male sex-dependent acceleration of islet senescence impairing β-cell function. This mouse model was developed on

a mixed genetic background of C57/Bl6J and SJL, thus efforts to backcross these mice on the C57 background were pursued in this report with the expectation that sex-dependent phenotypes would be maintained. Here we show that genetic background interacts with the MafA mutation to influence the prevalence of the male (moreso than female) dysfunction: male MafA^{S64F/+} mice on the C57/Bl6J prevented glucose intolerance and maintained glucose stimulated insulin secretion comparable to MafA^{WT} males. Breeding this C57 line just one generation to SJL mice recovered the diabetes phenotype in F1 MafA^{S64F/+} male progeny, highlighting either protective effects of the C57 background and/or prodiabetogenic effects of the SJL background. Comparing these mutant lines reveal attenuated β -cell senescence, increased *MafA* expression and presumed activity by target gene expression, and increased detection of a phosphorylated MafA species in the C57 background. Unbiased RNAseq analysis also uncovered a mixed genetic background-specific dysregulation of islet circadian regulators, identifying a novel link between β -cell maturity driver like MafA, cellular aging, and circadian entrainment.

Peripheral clock synchronization through entrainment is critical for coordinated metabolic responses such as maintaining euglycemia, and desynchronization of peripheral clocks in the absence of entraining signals can lead to metabolic derangement (*39*, *42*, *56*). The core clock transcriptional activators Clock and Bmal1 are produced in pancreatic islet β-cells and are essential for dynamic insulin secretion produced by oscillatory expression of genes encoding secretory machinery and factors regulating insulin release, such as Pdx1 and MafA itself (*36*, *37*). Ubiquitin ligases such as FBXL3/21 and TRCP1/2 subsequently regulate the periodicity of clock repressors Cry1/2 and Per1/2, respectively (*57-60*), akin to the regulatory posttranslational modifications required for turnover of Maf transcription factors (*1*). Ultimately, these processes newly link transcriptional output by MafA (such as *Insulin*), circadian rhythmicity and dynamic insulin secretion. Future studies to investigate whether MafA and these circadian regulators have ubiquitination mediators in common warrant further investigation.

Interestingly, we find that male *MafA*^{S64F/+} islets on the mixed background show marked downregulation of direct regulators *Per1*, *Per2*, *Cry2*, *Rora*, and *Rev-erb*, and amplification factors in complementary circadian circuits such as *Dbp* and *Nfil3* (**Fig. 6A**) (*61*). These signatures of circadian dysregulation is interesting as it results from *increased* levels of MafA, compared to known circadian disruption with the *deficiency* of another islet-enriched factor, Pdx1 (*36*). In addition to marked changes to islet gene expression, CUT&RUN analysis demonstrates that these circadian mediators are putative targets of β-cell MafA. Intriguingly, the core clock repressors identified here do not have MARE (MAF consensus) binding sites nor are

they recognized to bind MAFA/B in human islets (Islet regulome (62)). This suggests that while MAFA may not directly bind to these genes but may rather be a component of a scaffolding complex for other regulators to cooperatively bind. Indeed, we find differential SNPs within several genes encoding known MafA coregulators between the C57 and SJL backgrounds (**Supplemental Table 2**). These SNPS fell into the general categories of 3' or 4' UTR, downstream or upstream variants, intronic variants, or synonymous variant; none were potentially high impact missense variants. This suggests that contributions of multiple modifier(s) may contribute to MAFA regulation. Thus, careful forward genetic screens to identify other potential MafA co-regulators (such as ubiquitin ligases) distinct in the C57/Bl6J and SJL backgrounds are ongoing.

While the coexistence of dysregulated circadian entrainment and accelerated senescence is interesting, it is yet unclear whether these processes occur in parallel or along a common pathway to disturb insulin secretion. Genes encoding senescence regulators enriched in MafA^{S64F/+} males, such as p21 and Bcl2a1d, were not identified as having MafA occupancy by CUT&RUN, suggesting that circadian dysregulation may lie upstream to accelerating aging. Directed evaluation of β -cell senescence in models of disturbed circadian regulation would be fruitful, as would the evaluation of circadian dysregulation on other well-studied models of dysglycemia showing β -cell senescence, such as the NOD model (32) and in models of insulinresistance (31). Future efforts are needed to study the impact of MafA^{WT} and MafA^{S64F} on synchronized mice and cell systems on assess the integrity of the β -cell clock mechanisms.

We find that influence of C57/Bl6J and SJL backgrounds did not significantly impact the hypoglycemia and improved glucose tolerance of *MafA*^{S64F/+} females, suggesting a robust protective influence by the mutation itself over the modifying influence of genetic background and biologic sex. We previously showed by ovariectomy that postnatal estradiol did not principally drive the female glycemic pattern, and bulk RNAseq data and electrophysiological studies from these mouse islets showed significant changes in calcium handling across heterogenous islet populations. Heterogenous responses to MafA^{S64F}, particularly in females, warrant further investigation and allude to protective mechanisms of heightened MafA levels in specific contexts (i.e., female sex). Moreover, our studies here did not evaluate a possible protective effect of MafA^{S64F} in response to stressors such as glucolipotoxicity in high fat diet, and additional work may reveal protective effects of stable MafA^{S64F} in certain contexts.

Nevertheless, our work here demonstrates the combinatorial impact of genetic background and biologic sex on molecular and functional β-cell responses to produce heterogenous responses (i.e., cellular senescence driving dysfunction vs. hypoglycemia) to a

clinically relevant, stable variant of MafA. Our data here strongly suggest that additional regulators inherent in the C57/Bl6J and SJL backgrounds can "tune" the proportions of stable MafA^{S64F} and downstream responses and ultimately facilitate our ultimate goal to develop strategies to safely optimize β -cell function in people with diabetes.

Acknowledgements. This research was performed using resources and/or funding provided by NIH grants to JC (K08 DK132507), RS (R01 DK090570), ADA and MPK (R01DK101573, R01DK102948, and RC2DK125961) and by the Vanderbilt Diabetes Research and Training Center (DK20593). JC is also supported by a Burroughs Wellcome Fund Career Award for Medical Scientists, and MPK is also supported by University of Wisconsin-Madison Alumni Research Foundation. The authors thank the members of Rafael Arrojo e Drigo Lab (Vanderbilt University), and the Joseph Bass Lab (Northwestern University) for critical discussion, and Charles I. Opara for assistance in annotating the functional consequences of SNPs that are different between C57BL6/J and SJL/J.

Duality of Interest. No potential conflicts of interest relevant to this article were reported.

Author Contributions.

- ZL, DL, MM, MAM, RS, and JC designed the study.
- ZL, DL, MM, LB, JL, MG, GR, JPC, and JC performed experiments.
- ZL, DL, MM, LB, MPK, JPC, and JC performed bioinformatic analysis.
- ZL, DL, MM, LB, JL, MG, GR, MAM, MPK, JPC, RS, and JC analyzed data.
- ZL, DL, MM, RS and JC wrote the manuscript.
- ZL and DL are co–first authors due to their contributions in most of the experimental studies.

MAIN FIGURE LEGENDS

Figure 1. Glucose tolerance is largely unaffected in C57 MafA^{S64F/+} males, while those on a Mixed background manifest frank diabetes and impaired insulin secretion

A. Fasted male animals underwent intraperitoneal glucose tolerance tests at various time points as indicated. Male MafA^{S64F/+} heterozygous (termed "Het") mice on a C57 background had no changes to glucose tolerance through adulthood compared to MafA^{+/+} (termed "WT") male littermates

B. Fasted male animals underwent intraperitoneal glucose tolerance tests (GTT) at time points indicated. Het males on a Mixed background had impaired glucose tolerance by 5 weeks of age which then progressed to overt diabetes by 7 weeks of age.

C-D. Stimulated in vivo C-peptide (C) and insulin (D) measurements showed reduction in Het males at 5.5 weeks of age on a Mixed background. Two-tailed Student t test; *p < 0.05; **p < 0.01

E. Stimulated in vivo C-peptide measurements showed no significant changes between WT and Het males at 5.5 weeks of age on a C57 background

Figure 2. Phenotypic penetrance is largely unaffected in hypoglycemic MafA^{S64F/+} females between C57 and Mixed backgrounds.

A. Fasted female animals underwent intraperitoneal glucose tolerance tests at various time points as indicated. Female MafA^{S64F/+} heterozygous (termed "Het") mice on a C57 background had improved glucose tolerance through adulthood compared to MafA^{+/+} (termed "WT") female littermates

B. Fasted female animals underwent intraperitoneal glucose tolerance tests (GTT) at time points indicated. Het females on a Mixed background also showed improved glucose tolerance by 5 weeks of age.

C-D. Stimulated in vivo C-peptide (C) and insulin (D) measurements were similar between Het females at 5.5 weeks of age on a Mixed background. Two-tailed Student t test; *p < 0.05; **p < 0.01

E. Stimulated in vivo C-peptide measurements showed mild improvement in Het females at 5.5 weeks of age on a C57 background

Figure 3. Islet senescence is abrogated in MafA^{S64F/+} male islets on a C57 background.

A. Senescence associated beta gal staining (SA- β -gal) is enriched in male Het islets from the Mixed background, and qPCR of senescence signature genes are significantly altered in C57 islets at 5 weeks of age. *p < 0.05. Scale bar, 20 μ m.

- B. SA- β -gal staining not detectable in male Het islets from the C57 background, and qPCR of senescence signature genes are not enriched in C57 islets at 5 weeks of age. *p < 0.05
- C. Top, RNAScope for Cdkn1a encoding p21 shows enrichment in Het islets on a mixed background in β -cells. Bottom, Quantification of $Cdkn1a^{+}Ins^{+}$ cells. *p < 0.05
- D-E. Immunostaining of senescence markers show enrichment of 53BP1 and relative loss of nuclear LaminB1 in the mixed (D), but not C57 (E), background. Scale bar, $50\mu m$. Arrowhead, positive stain.

Figure 4. RNASeq shows improvement of global senescence signatures in islets of MafA^{S64F/+} C57 male islets compared to those of a mixed background

- A. Representative images of islet yields from each genotype and genetic background, with markedly paler islets and poorer yields in Het males on a mixed background
- B. Unbiased hierarchical clustering showed congruent organization within genotypes and genetic background
- C. Venn diagram illustrates the total number of RNA-seq-identified DEGs up- or down-regulated between 5-week-old WT and Het male islets of each background
- D. Heatmaps showing aging/senescence enrichment in Mixed, but not C57, Het male islets.

Figure 5. Deregulation of circadian rhythm pathway in MafA^{S64F/+} islets on a mixed, but not C57, background

- A. Gene Ontology (GO): molecular function analysis (p < 0.05) of the genes uniquely up- or down-regulated in each genetic background in male Het islets. Pathways associated with aging (protein digestion and absorption, calcium signaling, cell adhesion) are upregulated seen in both Mixed and C57 islets, but more significantly in the Mixed background. Pathways downregulated in each background were unique, including a novel finding of circadian rhythms.
- B. STRING analysis identified enrichment of pathways from DEG's identified from bulk RNASeq analysis, including proteoglycan and protein digestion, calcium signaling, neuroactive ligands and circadian rhythm.
- C. Left, Heatmap of differentially expressed circadian rhythm genes from bulk RNASeq analysis. Right, TPM counts of circadian rhythm genes showing downregulation in Het male islets of a Mixed, but not C57 background only. Two-tailed Student t test; *p < 0.05; **p < 0.01.

Figure 6. Overlay of MAFA Cut&Run peaks with differentially expressed genes unique only to C57 MafA^{S64F/+} or Mixed MafA^{S64F/+} males

A. DEGs identified uniquely in Male Het islets from a mixed background (1238 + 1114 = 2352 genes) versus those uniquely from a C57 background (228 + 855 = 1083 genes) were then overlayed with peaks identified by endogenous MafA CUT&RUN in mouse MIN6 cells (n=11403 peaks). Of these, 250 genes uniquely enriched in a C57 background overlapped with a MafA CUT&RUN peak, while 1210 were uniquely enriched in a Mixed background overlapped with a MafA CUT&RUN peak.

B. UCSC Genome Browser tracks showing genomic regions associated with endogenous MafA CUT&RUN peaks near known targets Ins1, Ins2, MafB, and Pdx1, and candidate genes Onecut1, Cry2, Per1, and Per2; MafA CUT&RUN enriched peaks are highlighted in dashed boxes, and regulated genes are depicted below IgG control tracks.

Figure 7. Phosphorylated MafA species are more preserved in islets of MafA^{S64F/+} C57 male islets compared to those from a mixed background

A-B. Immunostaining for MafA show poor detection in Mixed background male Het islets (left) but intact MafA in C57 male Het islets (right). Islets from MafA^{$\Delta\beta$} included as a negative control. Scale bar, 50 μ m.

C. Left lanes, Western blotting on MIN6 nuclear extract transfected to express either MAFA^{WT} or MAFA^{S64F} shows faster migration in mutant MAFA due to impaired posttranslational modification by phosphorylation. Right lanes, Isolated mouse islets from each genotype and background showed detectable levels of phosphorylated (active) MAFA in C57 background, but relative uniformity of MAFA species with impaired phosphorylation in the Mixed background.

D. Quantification of Western blotting bands by Line scan analysis shows greater proportion of phosphorylated MafA species (gray) in Het male islets from the C57 background compared to the Mixed background.

Figure 8. Deregulation of *MafA* in MafA^{S64F/+} islets on a mixed background

A. qPCR for *MafA*, *MafB*, *Ins1*, and *Pdx1* differs in Het male islets of mixed background (left) but largely intact in C57 Het males (right). *p < 0.05.

B. Immunostaining for Pdx1 across genotypes and backgrounds in male mice. Scale bar, 20um. Orange arrowheads, nuclear staining.

C. Immunostaining for MafB across genotypes and backgrounds in male mice. Scale bar, 50um. Green arrowheads, MafB⁺Ins⁺ cells.

SUPPLEMENTAL FIGURE AND TABLE LEGENDS

Supplemental Figure 1. Mixed background male and female MafA^{S64F/+} show hypoglycemia while nursing, extended wean does not impact hyperglycemia in Male Hets, and weight gain and insulin tolerance are similar between the genetic backgrounds

A. Random blood glucose monitoring at 2-3 weeks of age while nursing shows similar mild, transient hypoglycemia in Male and Female Het mice on a mixed background. *p < 0.05; **p < 0.01

- B. Random glucose level of suckling male Het mice on a mixed background at 5 weeks of age during an extended wean still reveals hyperglycemia, suggesting that the weaning process does not precipitate dysglycemia. *p < 0.05; **p < 0.01
- C-D. Weight gain as a proxy for overall health across genotypes, biologic sex, and age does not appear significantly altered between groups
- E. Insulin tolerance testing showing similar peripheral insulin sensitivity in male and female WT and Het mice on a mixed background.

Supplemental Figure 2. Islet senescence signatures are not seen in female Het islets of either background

A-B. qPCR of senescence signature genes are unchanged in Mixed (A) and C57 (B) background female MafA^{S64F/+} islets at 5 weeks of age.

Supplemental Figure 3. Nuclear localization of NF-kB is unchanged in MafA^{S64F/+} whole islets in both backgrounds.

A-B. Immunostaining showing similar proportions of nuclear NF-kB between C57 and Mixed background males at 5 weeks of age.

Supplemental Figure 4. Heatmaps of MafA target genes, coregulators and transcriptional regulators, and gel shift analysis shows that MAFA^{WT} and MAFA^{S64F} have similar binding of *Insulin1* enhancer.

- A. Heatmap of known MafA target genes from bulk RNASeg analysis.
- B. Gel shift assay of HeLa nuclear extract (NE) produced MAFA^{WT} and mutant MAFA^{S64F} bound to *INS* enhancer (known MAFA target), showing similar binding affinity. Specificity of MAFA binding showed by super shift (SS) with MafA antibody.
- C. Heatmap of known MafA co-regulators from bulk RNASeq analysis.
- E. Heatmap of known MafA transcriptional regulators from bulk RNASeq analysis.

Supplemental Table 1. Primer sequences and antibody sources

Supplemental Table 2. Differential SNPS between SJL and C57 genetic background mice in genes encoding MafA interacting proteins and their predicted consequences

Supplemental Table 3. Differential SNPS between SJL and C57 genetic background mice predicted to be missense mutations

REFERENCES

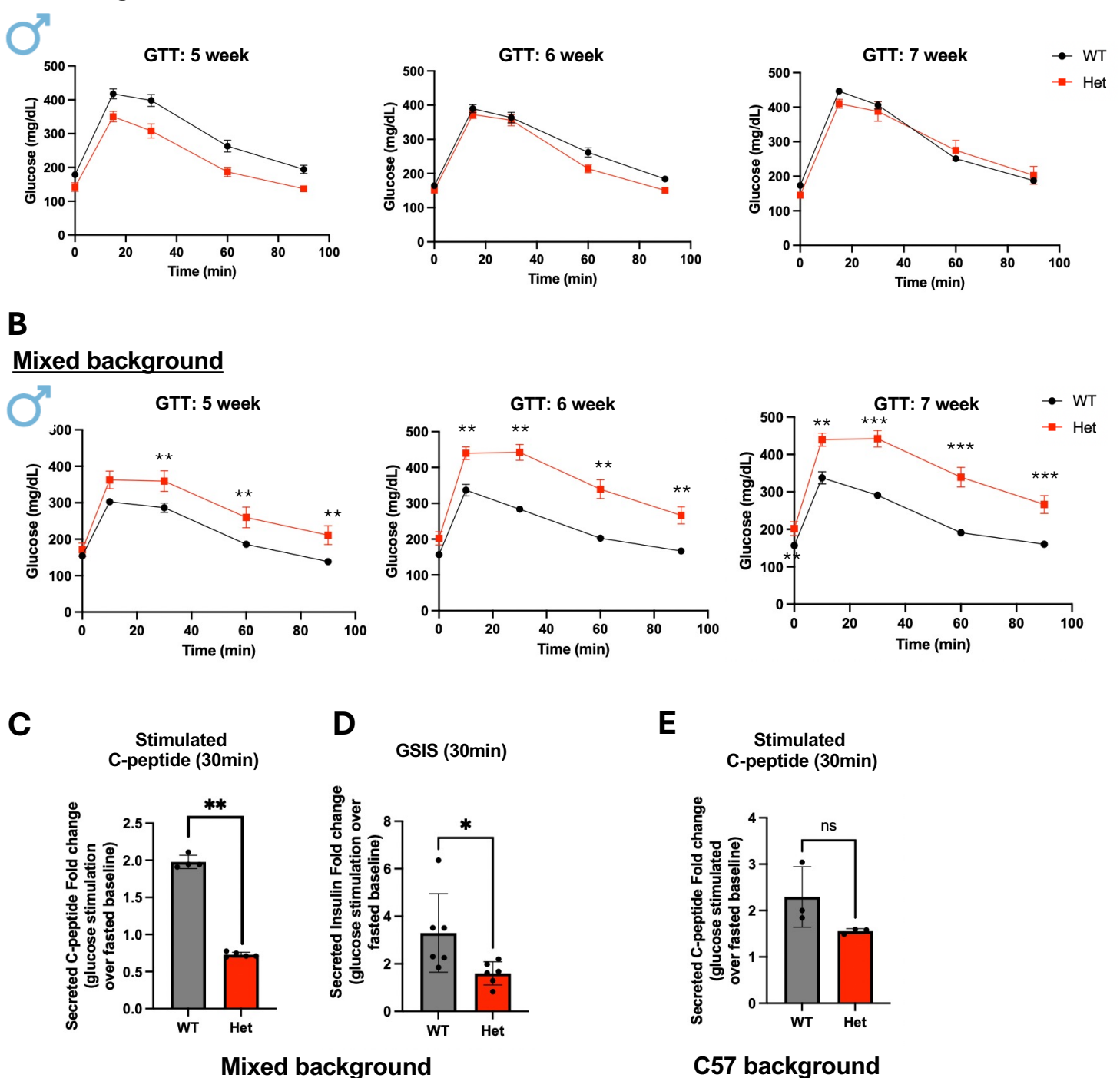
- 1. Y. Hang, R. Stein, MafA and MafB activity in pancreatic β cells. *Trends Endocrinol Metab* **22**, 364–373 (2011).
- 2. I. El Khattabi, A. Sharma, Proper activation of MafA is required for optimal differentiation and maturation of pancreatic beta-cells. *Best Pract Res Clin Endocrinol Metab* **29**, 821–831 (2015).
- 3. I. Artner, Y. Hang *et al.*, MafA and MafB regulate genes critical to β cells in a unique temporal manner. *Diabetes* **59**, 2530–2539 (2010).
- 4. H. A. Cyphert, E. M. Walker *et al.*, Examining how the MAFB transcription factor affects islet β cell function postnatally. *Diabetes* **68**, 337–348 (2019).
- 5. Y. Hang, T. Yamamoto *et al.*, The MafA transcription factor becomes essential to islet β cells soon after birth. *Diabetes* **63**, 1994–2005 (2014).
- 6. C. Zhang, T. Moriguchi *et al.*, MafA is a key regulator of glucose-stimulated insulin secretion. *Mol Cell Biol* **25**, 4969–4976 (2005).
- 7. C. Luan, Y. Ye *et al.*, The calcium channel subunit gamma-4 is regulated by MafA and necessary for pancreatic β cell specification. *Commun Biol* **2**, 106 (2019).
- 8. J. Cha, X. Tong *et al.*, Species-specific roles for the MAFA and MAFB transcription factors in regulating islet beta cell identity. *JCI Insight* **8**, (2023).
- 9. S. Guo, C. Dai *et al.*, Inactivation of specific β cell transcription factors in type 2 diabetes. *J Clin Invest* **123**, 3305–3316 (2013).
- 10. L. R. Cataldo, T. Singh *et al.*, MAFA and MAFB regulate exocytosis-related genes in human beta-cells. *Acta Physiol (Oxf)* **234**, e13761 (2022).
- 11. C. Aguayo-Mazzucato, A. Koh *et al.*, MafA expression enhances glucose-responsive insulin secretion in neonatal rat β cells. *Diabetologia* **54**, 583–593 (2011).
- 12. L. Wang, Y. Huang *et al.*, Differentiation of iPSCs into insulin-producing cells via adenoviral transfection of PDX-1, NeuroD1 and MafA. *Diabetes Res Clin Pract* **104**, 383–392 (2014).
- 13. A. Jeyagaran, M. Urbanczyk *et al.*, Forward programming of hiPSCs towards beta-like cells using Ngn3, Pdx1, and MafA. *Sci Rep* **14**, 13608 (2024).
- 14. A. Bonnefond, R. Unnikrishnan *et al.*, Monogenic diabetes. *Nat Rev Dis Primers* **9**, 12 (2023).
- 15. D. lacovazzo, S. E. Flanagan *et al.*, MAFA missense mutation causes familial insulinomatosis and diabetes mellitus. *Proc Natl Acad Sci U S A* **115**, 1027–1032 (2018).
- 16. E. M. Walker, J. Cha *et al.*, Sex-biased islet beta cell dysfunction is caused by the MODY MAFA S64F variant by inducing premature aging and senescence in males. *Cell Rep* **37**, 109813 (2021).
- 17. M. P. Keller, M. E. Rabaglia *et al.*, Gene loci associated with insulin secretion in islets from non-diabetic mice. *J Clin Invest* **129**, 4419–4432 (2019).
- 18. B. Marcheva, K. M. Ramsey *et al.*, Disruption of the clock components CLOCK and BMAL1 leads to hypoinsulinaemia and diabetes. *Nature* **466**, 627–631 (2010).
- 19. L. A. Sadacca, K. A. Lamia *et al.*, An intrinsic circadian clock of the pancreas is required for normal insulin release and glucose homeostasis in mice. *Diabetologia* **54**, 120–124 (2011).
- 20. J. Lee, M. Moulik *et al.*, Bmal1 and beta-cell clock are required for adaptation to circadian disruption, and their loss of function leads to oxidative stress-induced beta-cell failure in mice. *Mol Cell Biol* **33**, 2327–2338 (2013).
- 21. V. Petrenko, N. R. Gandasi *et al.*, In pancreatic islets from type 2 diabetes patients, the dampened circadian oscillators lead to reduced insulin and glucagon exocytosis. *Proc Natl Acad Sci U S A* **117**, 2484–2495 (2020).

- 22. J. A. Stamenkovic, A. H. Olsson *et al.*, Regulation of core clock genes in human islets. *Metabolism* **61**, 978–985 (2012).
- 23. J. Cha, X. Tong *et al.*, Defining unique structural features in the MAFA and MAFB transcription factors that control Insulin gene activity. *J Biol Chem*, 107938 (2024).
- 24. P. Bankhead, M. B. Loughrey *et al.*, QuPath: Open source software for digital pathology image analysis. *Sci Rep* **7**, 16878 (2017).
- 25. U. Schmidt, Weigert, M., Broaddus, C., Myers, G., Cell detection with star-convex polygons. *International Conference on Medical Image Computing and Computer-Assisted Intervention (MICCAI)*, (2018).
- 26. C. Benner, T. van der Meulen *et al.*, The transcriptional landscape of mouse beta cells compared to human beta cells reveals notable species differences in long non-coding RNA and protein-coding gene expression. *BMC Genomics* **15**, 620 (2014).
- 27. M. P. Meers, T. D. Bryson *et al.*, Improved CUT&RUN chromatin profiling tools. *Elife* **8**, (2019).
- 28. A. L. Lin, J.P. Cartailler, in *peakScout a user-friendly and reversible peak-to-gene translator for genomic peak calling results:* https://github.com/vandydata/peakScout. (2025).
- 29. Y. Song, in *ggcoverage Visualize* and annotate omics coverage with *ggplot2:* https://showteeth.github.io/ggcoverage/. (2025).
- 30. W. McLaren, L. Gil *et al.*, The Ensembl Variant Effect Predictor. *Genome Biol* **17**, 122 (2016).
- 31. C. Aguayo-Mazzucato, J. Andle *et al.*, Acceleration of β cell aging determines diabetes and senolysis improves disease outcomes. *Cell Metab* **30**, 129–142 e124 (2019).
- 32. P. J. Thompson, A. Shah *et al.*, Targeted elimination of senescent β cells prevents type 1 diabetes. *Cell Metab* **29**, 1045–1060 e1010 (2019).
- 33. J. Cha, C. Aguayo-Mazzucato, P. J. Thompson, Pancreatic beta-cell senescence in diabetes: mechanisms, markers and therapies. *Front Endocrinol (Lausanne)* **14**, 1212716 (2023).
- 34. P. Rorsman, M. O. Huising, The somatostatin-secreting pancreatic delta-cell in health and disease. *Nat Rev Endocrinol* **14**, 404–414 (2018).
- 35. P. Rodnoi, M. Rajkumar *et al.*, Neuropeptide Y expression marks partially differentiated beta cells in mice and humans. *JCI Insight* **2**, (2017).
- 36. B. J. Weidemann, B. Marcheva *et al.*, Repression of latent NF-kappaB enhancers by PDX1 regulates beta cell functional heterogeneity. *Cell Metab* **36**, 90–102 e107 (2024).
- 37. M. Perelis, B. Marcheva *et al.*, Pancreatic beta cell enhancers regulate rhythmic transcription of genes controlling insulin secretion. *Science* **350**, aac4250 (2015).
- 38. H. K. Hong, E. Maury *et al.*, Requirement for NF-kappaB in maintenance of molecular and behavioral circadian rhythms in mice. *Genes Dev* **32**, 1367–1379 (2018).
- 39. J. Bass, M. A. Lazar, Circadian time signatures of fitness and disease. *Science* **354**, 994–999 (2016).
- 40. K. Rakshit, J. Qian *et al.*, The islet circadian clock: entrainment mechanisms, function and role in glucose homeostasis. *Diabetes Obes Metab* **17 Suppl 1**, 115–122 (2015).
- 41. D. Szklarczyk, R. Kirsch *et al.*, The STRING database in 2023: protein-protein association networks and functional enrichment analyses for any sequenced genome of interest. *Nucleic Acids Res* **51**, D638–D646 (2023).
- 42. N. Seshadri, C. A. Doucette, Circadian Regulation of the Pancreatic Beta Cell. *Endocrinology* **162**, (2021).
- 43. J. Bass, J. S. Takahashi, Circadian integration of metabolism and energetics. *Science* **330**, 1349–1354 (2010).
- 44. M. Perelis, K. M. Ramsey *et al.*, Circadian Transcription from Beta Cell Function to Diabetes Pathophysiology. *J Biol Rhythms* **31**, 323–336 (2016).

- 45. M. Perelis, K. M. Ramsey, J. Bass, The molecular clock as a metabolic rheostat. *Diabetes Obes Metab* **17 Suppl 1**, 99–105 (2015).
- 46. W. Li, X. Xiong *et al.*, Transcription Repression of CRY2 via PER2 Interaction Promotes Adipogenesis. *Mol Cell Biol* **43**, 500–514 (2023).
- 47. K. Rakshit, A. V. Matveyenko, Induction of Core Circadian Clock Transcription Factor Bmal1 Enhances beta-Cell Function and Protects Against Obesity-Induced Glucose Intolerance. *Diabetes* **70**, 143–154 (2021).
- 48. N. Rocques, N. Abou Zeid *et al.*, GSK-3-mediated phosphorylation enhances Maftransforming activity. *Mol Cell* **28**, 584–597 (2007).
- 49. Y. Aida, K. Kataoka, CREB activates the MafA promoter through proximal E-boxes and a CCAAT motif in pancreatic beta-cells. *J Mol Endocrinol* **73**, (2024).
- 50. J. C. Raum, K. Gerrish *et al.*, FoxA2, Nkx2.2, and PDX-1 regulate islet beta-cell-specific mafA expression through conserved sequences located between base pairs -8118 and -7750 upstream from the transcription start site. *Mol Cell Biol* **26**, 5735–5743 (2006).
- 51. K. Yamamoto, T. A. Matsuoka *et al.*, A novel function of Onecut1 protein as a negative regulator of MafA gene expression. *J Biol Chem* **288**, 21648–21658 (2013).
- 52. D. B. Graham, C. E. Becker *et al.*, Functional genomics identifies negative regulatory nodes controlling phagocyte oxidative burst. *Nat Commun* **6**, 7838 (2015).
- 53. T. Cremer, M. L. M. Jongsma *et al.*, The ER-embedded UBE2J1/RNF26 ubiquitylation complex exerts spatiotemporal control over the endolysosomal pathway. *Cell Rep* **34**, 108659 (2021).
- 54. T. Manea, J. K. Nelson *et al.*, USP7 controls NGN3 stability and pancreatic endocrine lineage development. *Nat Commun* **14**, 2457 (2023).
- 55. C. Fottner, S. Sollfrank *et al.*, Second MAFA Variant Causing a Phosphorylation Defect in the Transactivation Domain and Familial Insulinomatosis. *Cancers (Basel)* **14**, (2022).
- 56. M. E. Hughes, L. DiTacchio *et al.*, Harmonics of circadian gene transcription in mammals. *PLoS Genet* **5**, e1000442 (2009).
- 57. K. Stojkovic, S. S. Wing, N. Cermakian, A central role for ubiquitination within a circadian clock protein modification code. *Front Mol Neurosci* **7**, 69 (2014).
- 58. A. Hirano, K. Yumimoto *et al.*, FBXL21 regulates oscillation of the circadian clock through ubiquitination and stabilization of cryptochromes. *Cell* **152**, 1106–1118 (2013).
- 59. S. H. Yoo, J. A. Mohawk *et al.*, Competing E3 ubiquitin ligases govern circadian periodicity by degradation of CRY in nucleus and cytoplasm. *Cell* **152**, 1091–1105 (2013).
- 60. K. Ohsaki, K. Oishi *et al.*, The role of beta-TrCP1 and beta-TrCP2 in circadian rhythm generation by mediating degradation of clock protein PER2. *J Biochem* **144**, 609–618 (2008).
- 61. Y. H. Kim, M. A. Lazar, Transcriptional Control of Circadian Rhythms and Metabolism: A Matter of Time and Space. *Endocr Rev* **41**, 707–732 (2020).
- 62. L. Pasquali, K. J. Gaulton *et al.*, Pancreatic islet enhancer clusters enriched in type 2 diabetes risk-associated variants. *Nat Genet* **46**, 136–143 (2014).

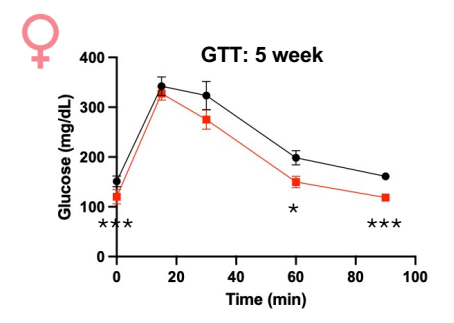


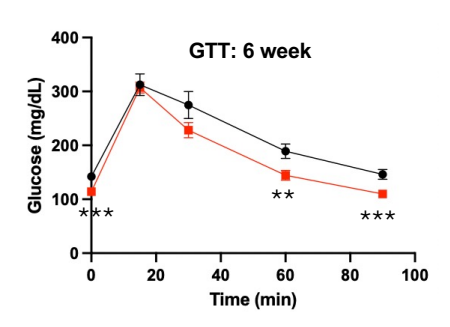
C57 background

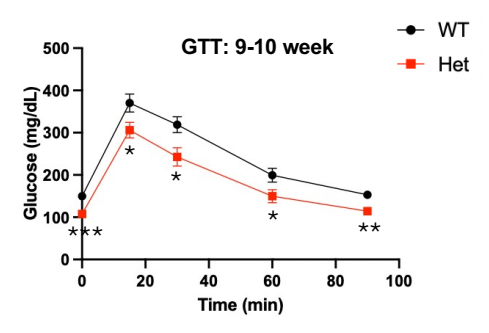




C57 background

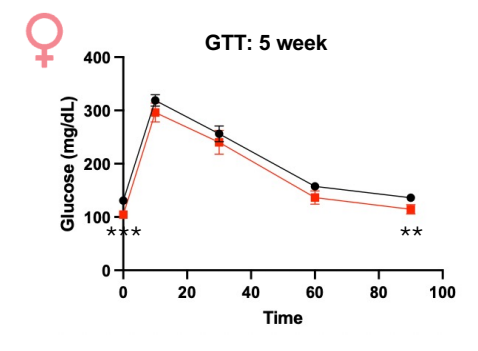


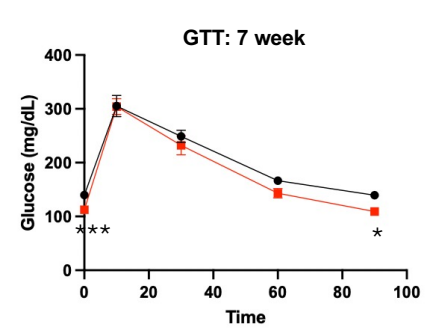


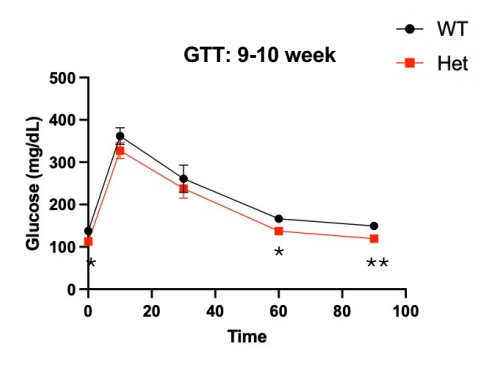


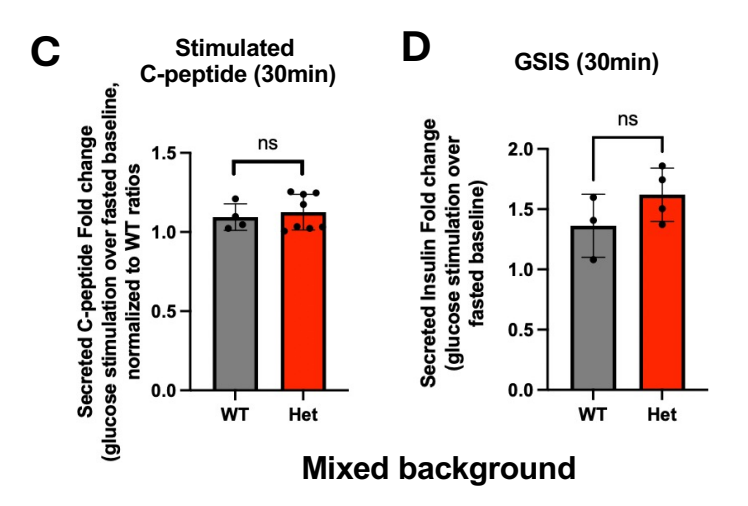
В

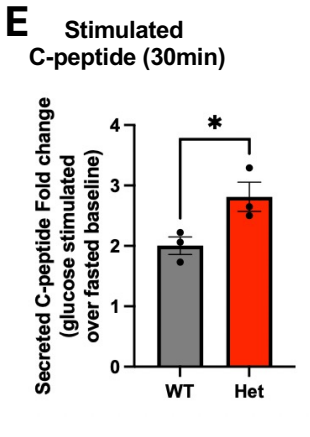
Mixed background



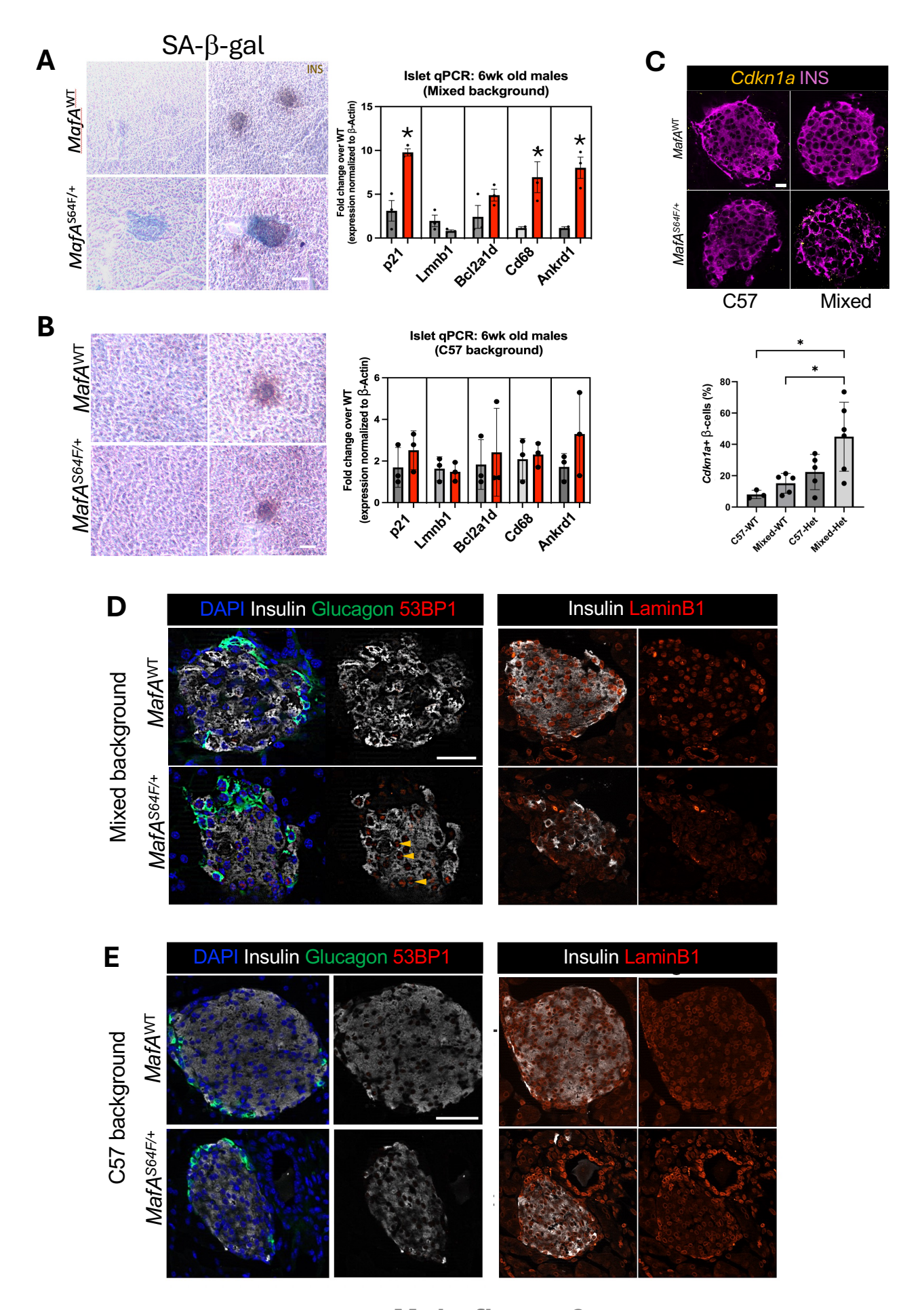








C57 background



Main figure 3

